Electronic and magnetic phase diagram of Sr_2FeO_4 at high pressure: A synchrotron Mössbauer study

Peter Adler[1,*] Sergey A. Medvedev[1] Qingge Mu[1] Dimitrios Bessas[2] Aleksandr Chumakov[2] Sergey Yaroslavtsev[2] Martin Jansen[1,3] and Claudia Felser[1]

[1]*Max-Planck-Institut für Chemische Physik fester Stoffe, 01187 Dresden, Germany*

[2]*ESRF–The European Synchrotron, CS 40220, 38043 Grenoble Cedex 9, France*

[3]*Max-Planck-Institut für Festkörperforschung, 70569 Stuttgart, Germany*

(Received 25 June 2024; revised 13 August 2024; accepted 14 August 2024; published 28 August 2024)

Transition metal (TM) oxides with high oxidation state TM ions exhibit a variety of unconventional electronic and magnetic states owing to electron correlations effects combined with highly covalent TM–O bonding. Here, we have studied the pressure dependence of electronic state and magnetism of the K_2NiF_4-type iron(IV) oxide Sr_2FeO_4 up to 89 GPa by temperature and magnetic field dependent energy-domain synchrotron Mössbauer spectroscopy and derived a (P,T) magnetic phase diagram. Considering also previous resistance studies [Rozenberg *et al.*, Phys. Rev. B **58**, 10283 (1998)] several magnetic and electronic regimes with increasing pressure can be identified. Near 7 GPa, the insulating cycloidal antiferromagnetic low-P state is transformed into a semiconducting ferromagnetic state and the magnetic ordering temperature T_m increases from 55 K at ambient pressure to about 100 K at 13 GPa. Between 18 and about 50 GPa the system is ferromagnetic and metallic (FMM) with a strong rise of T_m to above room temperature (RT). Contrary to a recent theoretical study [Kazemi-Moridani *et al.*, Phys. Rev. B **109**, 165146 (2024)], the FMM state is attributed to a high-spin $t_{2g}^3e_g^1$ electronic state with itinerant e_g coupled to more localized t_{2g} electrons. Between 50 and 89 GPa a doublet with large quadrupole splitting in the RT Mössbauer spectra indicates a partial high-spin to low-spin (t_{2g}^4) transition leading to a decrease in T_m again. The general features of the (P,T) phase diagram of Sr_2FeO_4 are comparable to those of other simple and A-site ordered iron(IV) perovskite-related oxides with the peculiarity that Sr_2FeO_4 adopts an insulating state without charge disproportionation of Fe^{4+} in the low-P region. The high-pressure behavior of Sr_2FeO_4 and other iron(IV) oxides may be relevant for exploring the role of Hund's physics in multiorbital systems and contributing to the understanding of the electronic situation in unconventional superconductors such as $La_3Ni_2O_7$ and Sr_2RuO_4.

DOI: 10.1103/PhysRevB.110.054444

I. INTRODUCTION

Transition metal (TM) oxides with TM ions in high oxidation states are frequently characterized by strong electron correlations as well as by pronounced covalency of transition metal–oxygen bonding. A very recent example for the unconventional properties emerging from this electronic situation is the observation of signatures for high-temperature superconductivity in the nickelate $La_3Ni_2O_7$ at high pressures above 14 GPa with a critical temperature T_c of 78 K, approaching the T_c values of cuprates [1]. Perovskite-related ferrates with iron in the oxidation state +IV present an example for this peculiar electronic regime. Within a generalized Zaanen-Sawatzky-Allen diagram [2] iron(IV) oxides, similar to Cu(III) oxides [3], have been described as compounds with negative effective charge-transfer energy (negative Δ) where both insulating as well as metallic electronic ground states are dominated by a $3d^5L^{-1}$ electron configuration with holes in the oxygen bands rather than by an ionic $3d^4$ configuration [4]. This scenario is supported by a photoemission study on $SrFeO_3$ [4] as well as by high energy x-ray diffraction experiments [5] which also confirm that the electronic ground state of Fe(IV) corresponds to a high-spin (HS) state. The latter formally arises from a $t_{2g}^3e_g^1$ ligand field configuration, but owing to the strong covalency of Fe-O bonding these orbitals are rather molecular orbitals with large contributions from O $2p$ orbitals. Iron(IV) oxides reveal a variety of unconventional electronic states such as a bad metal state in the cubic perovskite $SrFeO_3$ [6,7], charge disproportionation (CD) of Fe(IV) in $CaFeO_3$ [8,9] and in the Ruddlesden-Popper bilayer compound $Sr_3Fe_2O_7$ [10,11], and an insulating state without CD in the K_2NiF_4-type oxide Sr_2FeO_4 [12,13]. All these compounds exhibit antiferromagnetic order with spiral spin structures, irrespective of the actual electronic ground state [14,9,15,16]. The noncollinear magnetism is remarkable with respect to the recent interest in topological spin textures like skyrmions [17] which exhibit topological Hall effects and may lead to

*Contact author: adler@cpfs.mpg.de

Published by the American Physical Society under the terms of the Creative Commons Attribution 4.0 International license. Further distribution of this work must maintain attribution to the author(s) and the published article's title, journal citation, and DOI. Open access publication funded by Max Planck Society.

applications for data storage devices. Unconventional Hall effects have been observed for $SrFeO_3$ [18] and it has been suggested that $SrFeO_3$ hosts skyrmion- and hedgehoglike topological spin textures in spite of its centrosymmetric crystal structure which does not allow for the Dzyaloshinskii-Moriya interaction [19]. Also, $Sr_3Fe_2O_7$ exhibits a rich magnetic phase diagram with possibly complex spin textures [20]. Competing ferro- and antiferromagnetic interactions [14,15] or a pure double-exchange mechanism [21] were proposed as the origin for the spiral spin arrangements.

Insights into the interplay between charge, spin, and lattice degrees of freedom that determines the physical properties of iron(IV) oxides were obtained from high-pressure studies on several of the compounds. Nasu and co-workers performed comprehensive studies on $SrFeO_3$ up to 74 GPa employing temperature and field dependent laboratory as well as time-domain synchrotron [nuclear forward scattering (NFS)] ^{57}Fe Mössbauer experiments [22–28]. Notably, the ambient-pressure helical spin structure of $SrFeO_3$ starts to transform into a high-pressure ferromagnetic spin structure near 7 GPa which persists up to 74 GPa. The change in spin structure is accompanied by a huge increase in the magnetic ordering temperature from 134 K at ambient pressure to well above room temperature for pressures larger than 20 GPa. It was verified by x-ray diffraction (XRD) studies that the cubic crystal structure is retained at least up to 56 GPa [29]. A more complex (P,T) phase diagram was obtained for $CaFeO_3$, which is the prototypical system where Fe(IV) features a charge disproportionation ($2 \cdot 3d^4 \rightarrow 3d^5 + 3d^3$ or $2 \cdot 3d^5L^{-1} \rightarrow 3d^5 + 3d^5L^{-2}$ within the negative-Δ scenario) in the paramagnetic phase below $T_{CD} = 290\,K$ as well as in the helical antiferromagnetic phase below $T_N = 115\,K$ [8,9]. The CD state is suppressed near 20 GPa and above 30 GPa a room-temperature (RT) ferromagnetic phase emerges [30,31] which has been attributed to a low-spin (LS) Fe(IV) state. The electronic structure change at 30 GPa is associated with a structural change though the high-pressure crystal structure is still elusive. Similar to $CaFeO_3$, also the CD in $Sr_3Fe_2O_7$ is suppressed near 20 GPa, where a change from insulating to metallic behavior without apparent structural anomalies up to 45 GPa was found [32]. Pressure-induced suppression of CD was also reported for A-site ordered perovskites $ACu_3Fe_4O_{12}$ with $A = Ca$, Sr where for $A = Sr$ in addition pressure-induced intersite charge transfer occurs [33,34]. Most remarkably, a HS→LS transition beyond 30 GPa was established in these compounds.

The present work deals with the high-pressure magnetism and electronic state of Sr_2FeO_4, which is an antiferromagnetic insulator ($T_N = 56\,K$) at ambient pressure but without CD of Fe(IV) [12,13]. Sr_2FeO_4 crystallizes in the K_2NiF_4-type crystal structure with single perovskitelike iron-oxygen layers separated by SrO rocksalt-like layers. Previous XRD and neutron diffraction data were refined within the tetragonal space group $I4/mmm$ [35,12], but ambient-pressure Raman spectra revealed an oxygen-phonon mode that is not intrinsic to the $I4/mmm$ structure [36,16] and may indicate a hidden structural instability stabilizing the insulating ground state. Recently, a theoretical study predicted symmetry lowering in Sr_2FeO_4 arising from Jahn-Teller distortion [37]. At ambient pressure, Sr_2FeO_4 adopts an elliptically modulated cycloidal spin structure with the spins predominantly oriented in the ab plane, which is the origin of the complex Mössbauer spectra with a broad distribution of hyperfine fields [16]. Earlier high-pressure studies of Sr_2FeO_4 have shown that the apparent tetragonal crystal structure is retained up to at least 30 GPa [38], while the additional Raman band is suppressed above 6 GPa [36]. At similar pressures a drop of the electrical resistance by several orders of magnitude was reported but the compound remained semiconducting up to 18 GPa, where metallic behavior emerged [38]. In contrast to the low-pressure region, $P \leqslant 7$ GPa, a simple six-line pattern was found in the low-temperature Mössbauer spectrum at 19 GPa, i.e., in the metallic region. This indicates a pressure-driven change in spin structure, but the critical pressure for the transformation was not reported and the nature of the high-pressure magnetic state was not established. The pressure-induced changes in electronic and magnetic properties were attributed to the closure of the p-p type gap in the insulating negative-Δ ground state [38]. Recently, the ambient and high-pressure electronic behavior of Sr_2FeO_4 in the paramagnetic phase was studied using a combination of density functional theory (DFT) and dynamic mean field theory (DMFT) [39]. It was proposed that the metallic high-pressure state of Sr_2FeO_4 could resemble the electronic state of the unconventional metal and superconductor Sr_2RuO_4.

In order to elaborate details of the electronic and magnetic (P,T) phase diagram of Sr_2FeO_4 and to extend the pressure range beyond 30 GPa, we have investigated Sr_2FeO_4 by temperature and field dependent synchrotron Mössbauer spectroscopy at pressures up to 89 GPa, using the synchrotron Mössbauer source (SMS) at the European Synchrotron Radiation Facility (ESRF) [40] to collect energy-domain Mössbauer spectra. As we have briefly shown already in Ref. [16], a transformation from the low-pressure spiral to a ferromagnetic spin structure occurs between 5 and 8 GPa, which is just the pressure range where the additional Raman phonon disappears, but well below the metallization pressure of 18 GPa. Here, we report the results of a comprehensive high-pressure SMS study with emphasis on field dependent measurements to clarify the nature of the magnetic states and on the exploration of the high-pressure magnetism and electronic states beyond 20 GPa.

II. EXPERIMENTAL DETAILS

Sr_2FeO_4 was synthesized from SrO and Fe_2O_3 powder which was enriched in the isotope ^{57}Fe as described previously [16]. Most of the high-pressure experiments were performed with a sample that was enriched to 20% ^{57}Fe. Ambient-pressure Mössbauer spectra of the sample confirmed the high degree of oxidation of iron and the estimated composition is $Sr_2FeO_{3.99(1)}$. The experiments at 5 and 12 GPa were performed with a sample that was enriched to 10% ^{57}Fe and revealed a slightly higher oxygen deficiency of about 0.02 as estimated from its ambient-pressure Mössbauer spectra at low temperature.

Energy-domain Mössbauer spectra at pressures up to 89 GPa were recorded in diamond-anvil cells (DACs) manufactured from the nonmagnetic alloy MP35N using the synchrotron Mössbauer source [40] at beamline ID18 of

ESRF [41], Grenoble. DACs equipped with 500- and 300-μm Boehler-Almax design diamond anvils have been used to generate pressures below 50 GPa and up to ∼90 GPa, respectively. The powder samples of Sr_2FeO_4 were loaded in the sample chambers of 200 (100) μm diameter and a thickness of ∼40 (∼25) μm, preindented into a tungsten gasket, with silicone oil as the pressure-transmitting medium. The DACs were prepared prior to the beamtime in the home laboratory in a glovebox with an Ar atmosphere with O_2 and H_2O content below 0.1 ppm. After the loading, the pressure in the DAC was increased to the target value. The pressure was determined by the ruby luminescence method (below 50 GPa) and by pressure shift of the Raman band of the stressed diamond anvil (above 50 GPa) before and after the temperature dependent synchrotron studies. For some of the runs, differences of pressure before and after temperature cycle up to 3 GPa were found. In these cases, the latter pressure was used for labeling the samples. After the synchrotron studies the samples in the DACs were characterized at room temperature by Raman spectroscopy. Raman spectra were recorded using a customary confocal micro-Raman spectrometer with a HeNe laser as the excitation source and a single-grating spectrograph with 1 cm^{-1} resolution.

For temperature and magnetic field dependent synchrotron Mössbauer studies, the DACs were placed into a cryomagnetic system from CryoIndustries. The beam size of the SMS radiation was about 10 × 10 μm^2. The velocity scale was calibrated with a 25-μm natural α-iron foil and the linewidth and center shift of the SMS were determined by measuring the spectra of the single line absorber $K_2Mg^{57}Fe(CN)_6$ having an intrinsic linewidth of 0.21 mm/s, after the collection of each sample spectrum. At several pressures, spectra with external magnetic fields $\boldsymbol{B}_{ext}$ were measured, where the field was either applied along the x-ray beam direction (longitudinal field) or perpendicular to the x-ray beam direction and parallel to the electric field vector $\boldsymbol{e}$ of the linearly polarized x rays (vertical field). Note that the SMS changes the direction of $\boldsymbol{e}$ from the initial horizontal to the vertical plane. The SMS spectra were evaluated with the program MOSSWINN [42], version 4.0i, using the transmission integral and a squared Lorentzian for the source function. The isomer shifts are referenced to α iron at room temperature. Some low-temperature SMS spectra in the antiferromagnetic phase were also analyzed using the model of anharmonic spin modulation [43] which was implemented into the SYNCMOSS software [44].

III. RESULTS

Previous XRD measurements confirmed that the ambient-pressure apparent tetragonal crystal structure is stable up to at least 30 GPa [38]. To characterize the samples structurally, the Raman spectra of the samples have been measured at RT after the SMS experiments (Supplemental Material Fig. S1 [45]). Spectra at the low pressures are in good agreement with the previous Raman studies. Notably, at low pressures (1 and 5 GPa), unexpected for the *I*4/*mmm* crystal structure, a broad band near 350 cm^{-1} is observed, which has been shown to sharpen upon cooling and which is suppressed above 6 GPa [36,16]. Although the spectra become increasingly broad with increasing P and are disturbed by strong luminescence from the stressed diamond anvils, the main bands are still discernible indicating that the tetragonal crystal structure is retained up to at least 51 GPa. At even higher pressures (65 and 71 GPa) the band near 700 cm^{-1} corresponding to the totally symmetric oxygen-phonon mode demonstrates strong asymmetry. In the absence of direct crystal structure studies at these pressures, it cannot be decided whether this is due to pressure inhomogeneities or indicates the coexistence of two phases with inequivalent crystal structures as suggested by the Mössbauer spectra (see below).

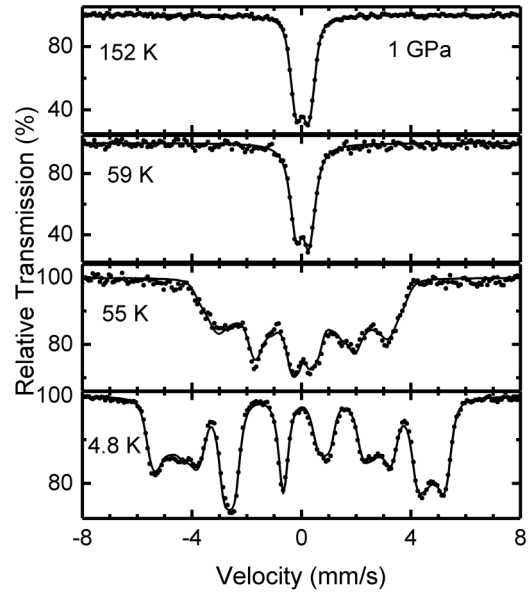

FIG. 1. SMS spectra of Sr_2FeO_4 at 1 GPa and the indicated temperatures. Dots correspond to the experimental data and solid lines are calculated spectra which were obtained using a hyperfine field distribution in the magnetically ordered state or a quadrupole doublet in the paramagnetic state.

The SMS spectra at 1 GPa (Fig. 1) are in good agreement with the ambient-pressure Mössbauer spectra of the sample presented earlier [16]. The most prominent feature is the complex shape of the spectra in the magnetically ordered phase which can be fitted by extracting a hyperfine field (B_{hf}) distribution and assuming a linear correlation between B_{hf} and the quadrupole-coupling parameter ε. The distribution essentially reflects the pronounced modulation of the magnetic moments that is associated with the elliptical cycloidal spin structure [46,16]. From powder neutron diffraction studies a propagation vector ($\tau\tau 0$) with $\tau = 0.137$ was obtained. The magnetic moments are aligned essentially in the *ab* plane of the tetragonal crystal structure but a certain tilting against the *c* axis cannot be excluded. The latter has been considered to be the origin for the correlation between ε and B_{hf}, which implies that the angle θ between B_{hf} and the principal axis V_{ZZ} of the electric field gradient (EFG) tensor varies within the spiral spin structure [$2\varepsilon = (eQV_{ZZ}/4)(3\cos^2\theta - 1)$ for an axially symmetric EFG, where Q is the quadrupolar moment of the $I = 3/2$ excited nuclear state]. For space group *I*4/*mmm*, one could expect that V_{ZZ} is aligned along the tetragonal *c* axis; however, the actual crystal symmetry may be lowered by Jahn-Teller type distortions [37] that could lead to different

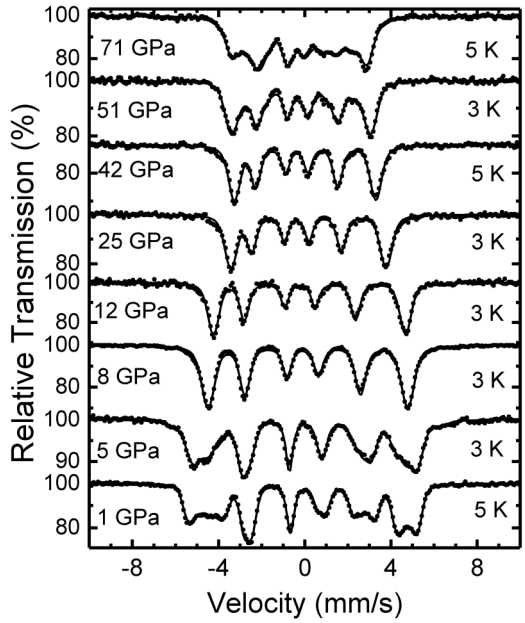

FIG. 2. SMS spectra of Sr_2FeO_4 at low temperatures at the indicated pressures. Dots correspond to the experimental data and solid lines are calculated spectra (see text for discussion of the data evaluation).

Fe-O distances in the *ab* plane and thus a different orientation of V_{ZZ}. The spectra indicate a magnetic ordering temperature of about 56 K, similar to that at ambient pressure. In the paramagnetic phase the spectra consist of a simple quadrupole doublet (quadrupole splitting QS = 0.44 mm/s at 152 K).

In Fig. 2 the evolution of the low-temperature SMS spectra (3–5 K) with pressure up to 71 GPa is shown. At 5 GPa the spectrum still exhibits a complex B_{hf} distribution though its detailed shape is somewhat modified compared to the spectrum collected at 1 GPa. It is concluded that at 5 GPa still a complex spin texture is present. On the other hand, at 8 GPa the complex shape of the spectrum has vanished and only a single six-line pattern is observed. As we have shown already in Ref. [16], a longitudinal magnetic field of 2 T leads to a decrease of B_{hf} by about 1.4 T suggesting ferromagnetic spin alignment.

More comprehensive sets of field dependent SMS spectra with vertical magnetic fields up to 7.9 T and with $\boldsymbol{B}_{ext}$ parallel to $\boldsymbol{e}$ were obtained at 1 and 13 GPa, respectively. The response of the spectral shapes to $\boldsymbol{B}_{ext}$ is very different at the two pressures (Fig. 3). At 1 GPa a complex shape of the spectra is retained up to 7.9 T and the average B_{hf} of the B_{hf} distribution is nearly independent of B_{ext} (Fig. 4). As in the case of the zero-field spectra, we have first fitted the spectra with a B_{hf} distribution where ε was assumed to correlate linearly with B_{hf}. While the width of the signals was reproduced quite well, a significant deviation between calculated and experimental spectra became apparent above 2 T. The cycloidal magnetic state of Sr_2FeO_4 corresponds to a spatially modulated spin structure. To describe its dependence on an external magnetic field we have fitted the spectra using the anharmonic spin modulation (ASM) model for a cycloidal spin

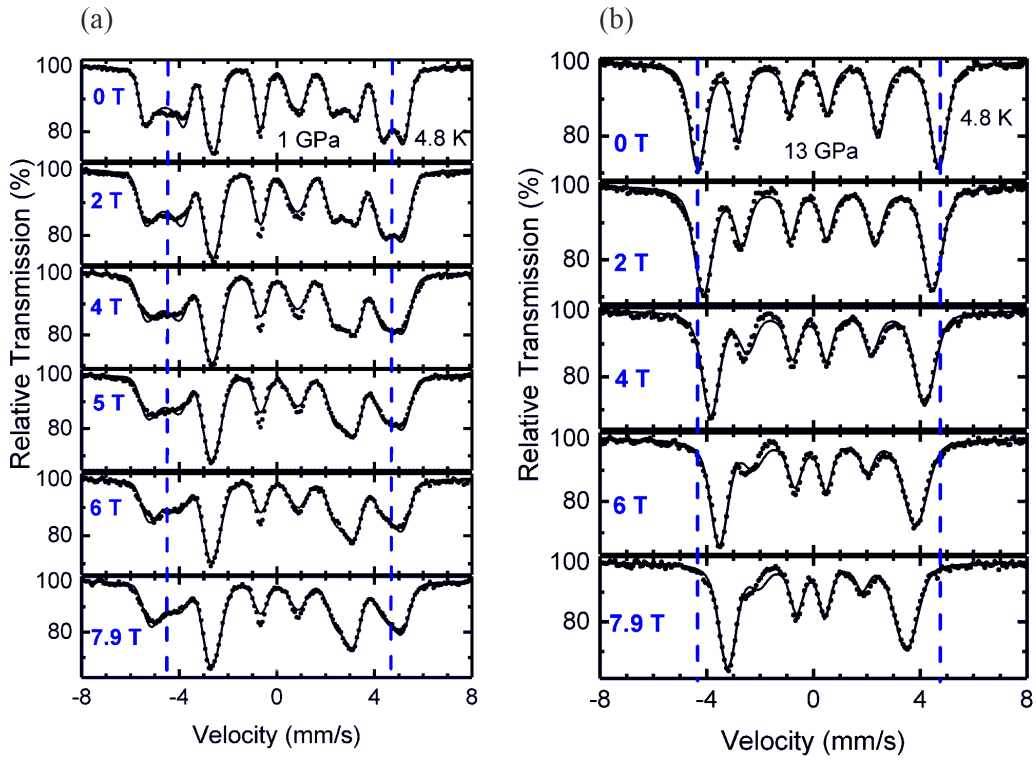

FIG. 3. Field dependent SMS spectra of Sr_2FeO_4 at 4.8 K at (a) 1 GPa and (b) 13 GPa. Dots correspond to the experimental data and solid lines are calculated spectra, where the spectra in (a) were evaluated within the ASM model and in (b) a hyperfine field distribution was used. The dashed lines indicate the average B_{hf} at zero field. The external fields were applied perpendicular to the x-ray beam direction and parallel to the electric field vector $\boldsymbol{e}$.

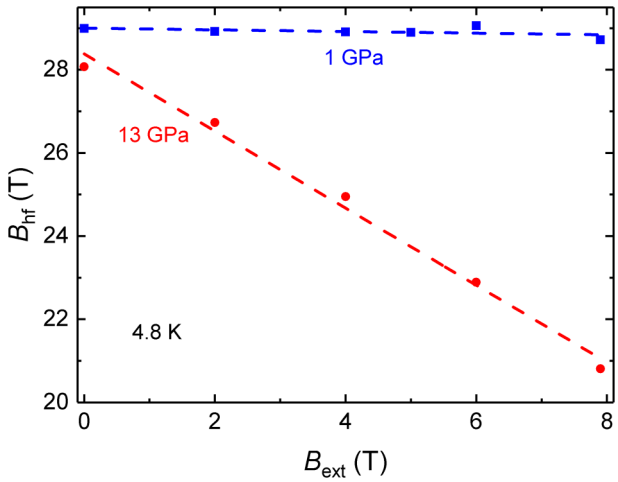

FIG. 4. Dependence of the average hyperfine field B_{hf} of the SMS spectra of Sr_2FeO_4 at 4.8 K on external magnetic field B_{ext} at 1 and 13 GPa, respectively. Dashed lines are guides to the eye.

structure [43,47–49] which was implemented into the SYNCMOSS software [44]. More details about the ASM evaluation are given in Ref. [45]. The applicability of the ASM model was verified by fitting the ambient-pressure laboratory Mössbauer spectrum (Fig. S2 [45]) although the actual B_{hf} distribution reveals some more structure in between the maxima at the edges [16]. The broad B_{hf} distribution within the ASM model is due to a large anisotropic contribution B_{an} to B_{hf} of about 6 T which is attributed to dipolar field contributions [12] and the pronounced modulation of magnetic moments in the elliptical spin structure [16]. The evolution of the shape of the SMS spectra with magnetic field can be well reproduced within the ASM model [Fig. 3(a)] and is reflected in an enhanced intensity of the nuclear transitions with $\Delta m_I = 0$ (corresponding to lines 2 and 5 in a single six-line pattern), and a strong increase in the anharmonicity parameter m between 3 and 6 T (see Fig. S3 [45]). These changes are attributed to a spin-flop (SF) -like transition leading to a reorientation of the spin ellipses which was found to occur near 5 T at ambient pressure [16]. The SF transition leads to a preferred orientation of moments perpendicular to $\boldsymbol{B}_{ext}$ and bunching of moments which is reflected in the shape of the Mössbauer spectra.

By contrast, the relative intensity of lines 2 and 5 in the simple sextet at 13 GPa is continuously reduced and B_{hf} decreases nearly linearly with B_{ext} (Fig. 4). Altogether, these results verify that between 5 and 8 GPa a transition from an antiferromagnetic spiral spin structure to a ferromagnetic type spin alignment occurs. Remarkably, lines 2 and 5 do not vanish completely in the spectra at 13 GPa, not even at 7.9 T, indicating that the ferromagnetic spin alignment is not complete. Furthermore, with increasing B_{ext} an asymmetric line shape with considerable broadening of the high-velocity component emerges. The line broadening can be partly reproduced by fitting the spectra assuming a B_{hf} distribution with linear correlation between B_{hf} and ε. However, this model does not reproduce an apparent decrease in the distance between lines 1 and 2 with increasing B_{ext}. The asymmetry in the spectra is possibly related to pronounced anisotropy arising from the tetragonal (or lower) crystal symmetry which prevents full ferromagnetic alignment of spins and may also be the origin of line shifts.

The single six-line pattern at low temperatures persists up to about 51 GPa (Fig. 2), where in addition a component with lower B_{hf} emerges. The average hyperfine field of the six-line pattern shows a discontinuity near the anticipated metallization pressure of 18 GPa [38] and decreases from 29 T at 8 GPa to 20 T at 51 GPa [Fig. 5(a)]. The isomer shift decreases with increasing P. Beyond 60 GPa the shape of the spectra becomes considerably more complex. We have analyzed the spectra by assuming a single six-line outer component and an additional component with a hyperfine field distribution which is characterized by a smaller average B_{hf}. The B_{hf} value of the outer compound is only slightly smaller than the B_{hf} values at 42 and 51 GPa [Fig. 5(a)], suggesting that it corresponds to a persisting ferromagnetic and metallic (FMM) phase. This clue is supported by SMS spectra that were measured at 65 GPa and 4.8 K in transverse magnetic fields (Fig. 6). While it is still difficult to decompose the spectra into components, it is obvious that B_{hf} of the outer component decreases with increasing B_{ext}, similar as in the spectra at 13 GPa (Fig. 3).

More insights into the changes in the electronic and magnetic properties with pressure are obtained from the spectra measured near RT, which are shown in Fig. 7. The RT spectra up to 12 GPa consist of a quadrupole doublet with small QS while the spectrum at 25 GPa is dominated by a magnetic hyperfine pattern in addition to a minor component attributed to a collapsing hyperfine pattern. The RT spectrum of another cell with P near 25 GPa exhibiting only slightly different (P,T) conditions features the coexistence of paramagnetic and magnetically ordered phases (Fig. S4 [45]), while the spectrum at 42 GPa reveals well-developed magnetic order for the whole sample. These results demonstrate that the magnetic ordering temperature T_m has drastically increased to near RT at 25 GPa and beyond RT at even higher pressures. However, at 51 GPa the spectrum reveals a considerable fraction of a component with small B_{hf} again, indicating the presence of a component with decreased T_m. Beyond 60 GPa, the average T_m has decreased to below RT and the RT spectra do not reveal well-resolved magnetic hyperfine splitting anymore. Most remarkably, a paramagnetic component with large QS emerges. For instance, the spectrum at 71 GPa (Fig. 7) features a doublet component with QS$\sim$1.2 mm/s, in addition to a broad signal attributed to a collapsing hyperfine pattern. A well-defined quadrupole doublet with isomer shift, IS $= -0.41$ mm/s, and QS $= 1.27$ mm/s was observed at 89 GPa, the highest pressure achieved within this study.

More details about the temperature range of magnetic ordering were obtained from the temperature dependence of the SMS spectra at different pressures, which is shown in Figs. 8, 9, and S6 [45]. The spectra typically are characterized by a broad coexistence range of magnetically ordered and collapsing or paramagnetic phase. Thus, it is not possible to derive a well-defined T_m for the high-pressure phases. To characterize the magnetic ordering behavior we use as an estimate for the average T_m the temperature where the fraction of magnetically ordered and collapsed phases were approximately equal in the spectra. In the low-pressure range T_m increases quite smoothly from 56 K at 1 GPa to $\sim$100 K at 13 GPa, where the system

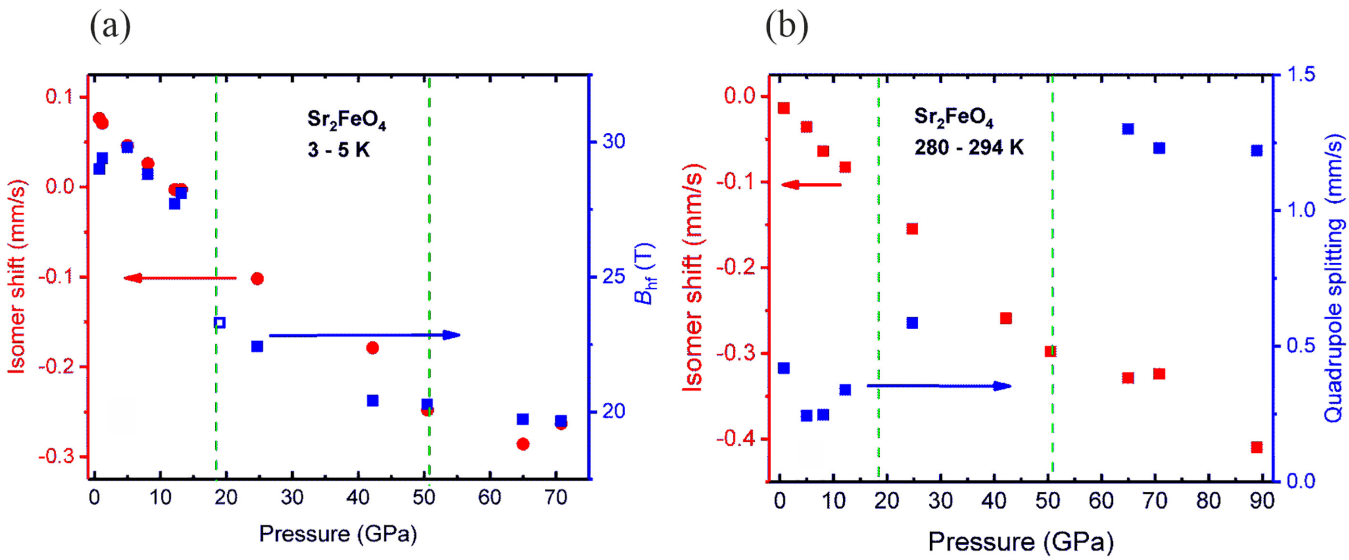

FIG. 5. Pressure dependence of the Mössbauer parameters obtained from the evaluation of the SMS spectra of Sr_2FeO_4. (a) Pressure dependence of isomer shift (red, left scale) and hyperfine field (blue, right scale; open symbol: data point from Ref. [38]) at low temperatures. For 65 and 71 GPa only the B_{hf} values of the outer component in the corresponding spectra are shown (see Figs. 2 and 6). (b) Pressure dependence of the isomer shift (red, left scale) and quadrupole splitting (blue, right scale,) near room temperature. Note that at 42 and 51 GPa no values of the quadrupole splitting are given as the magnetic order persists at room temperature and the orientation between the electric field gradient and the magnetic hyperfine field cannot be derived unambiguously. The vertical dashed lines mark the pressure of metallization (18 GPa) according to Ref. [38] and the pressure above which the SMS spectra indicate a partial HS→LS transition.

is still semiconducting [38]. As seen from the RT spectra, T_m increases to beyond RT near 40 GPa, but it decreases again to below RT beyond 50 GPa. In contrast to 42 GPa, only part of the sample is magnetically ordered at 51 GPa and RT, whereas an additional component with small average B_{hf} is apparent. The area fraction of the latter does not change much between

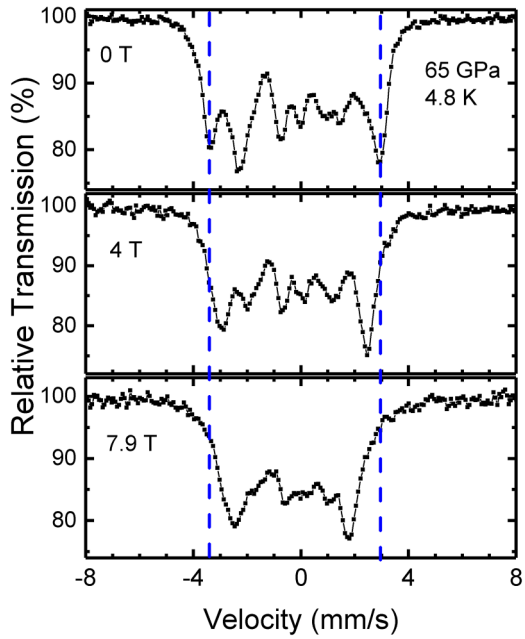

FIG. 6. Field dependent SMS spectra of Sr_2FeO_4 at 4.8 K at 65 GPa. Dots correspond to the experimental data and solid lines here are guides to the eye, not calculated spectra. The vertical dashed lines indicate the average B_{hf} of the outer component at zero field.

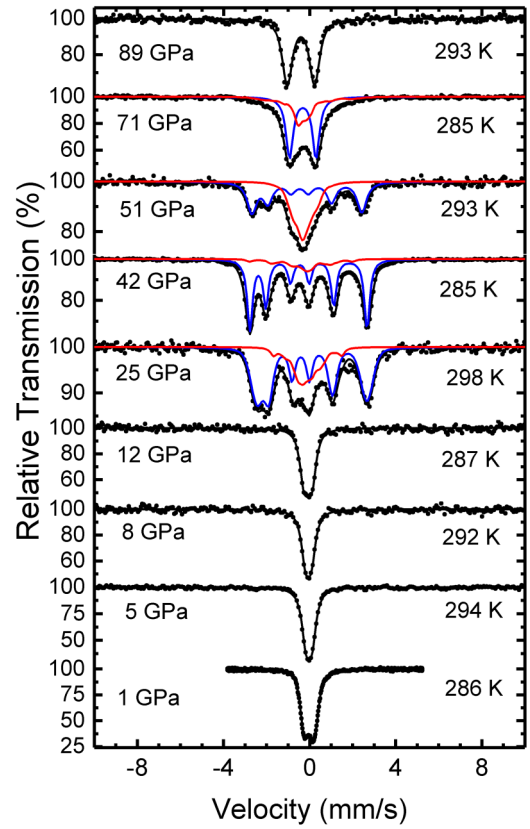

FIG. 7. SMS spectra of Sr_2FeO_4 near room temperature at the indicated pressures. Dots correspond to the experimental data, solid lines are calculated spectra, and colored lines correspond to the subspectra.

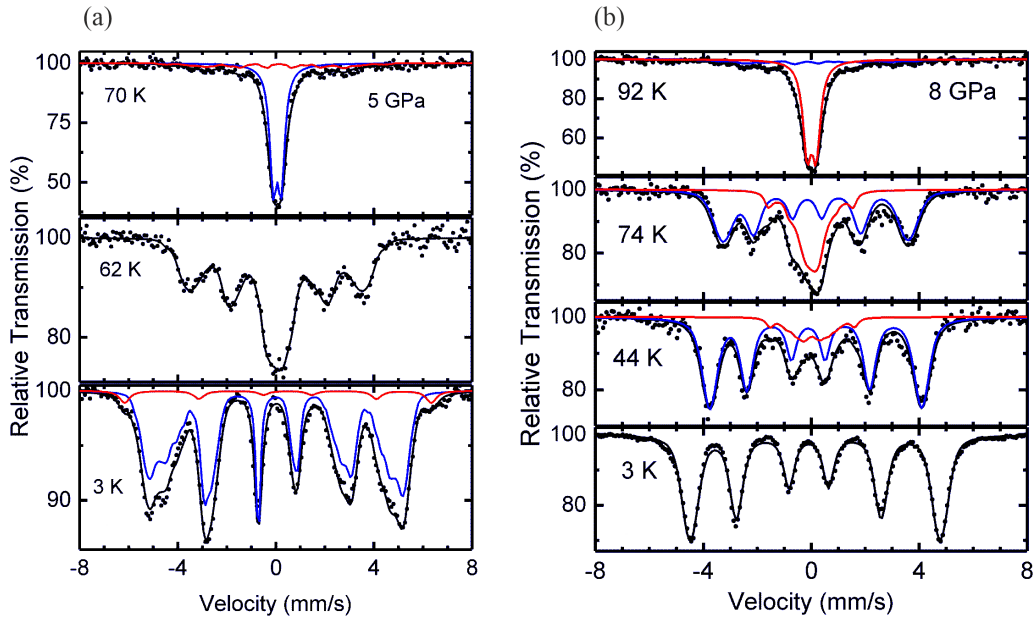

FIG. 8. Temperature dependence of the SMS spectra at (a) 5 and (b) 8 GPa. Dots correspond to the experimental data, solid lines are the calculated spectra, and colored lines correspond to the subspectra. The spectrum at 5 GPa and 3 K was fitted assuming a B_{hf} distribution; the minority component is attributed to a Fe^{3+} component. An alternative fit of the latter spectrum using the ASM model is provided in Fig. S5 [45].

200 and 293 K [Fig. 9(a)] and seems to fully order only below 150 K. An inhomogeneous magnetic state is also suggested by the low-T spectrum at 51 GPa, which cannot be fitted by a single sextet.

Our data indicate that beyond 50 GPa an electronic/structural phase transition takes place, which is reflected in the appearance of a quadrupole doublet with large QS at RT in the spectra at 65 and 71 GPa. The doublet appears to be the only component in the 89-GPa spectrum suggesting that the phase transition is complete. Unfortunately, we could not follow the T dependence of the spectra at 89 GPa as the diamond anvils failed upon cooling. At 65 and 71 GPa the T dependence of the spectra is complex owing to the coexistence of phases with different T_m [Figs. 9(b) and S6 [45]], and it is difficult to provide an unambiguous analysis of the spectra. Possibly one fraction of the samples orders around 250 K in this pressure range and another one at somewhat lower temperature, but it is likely that there are distributions in T_m

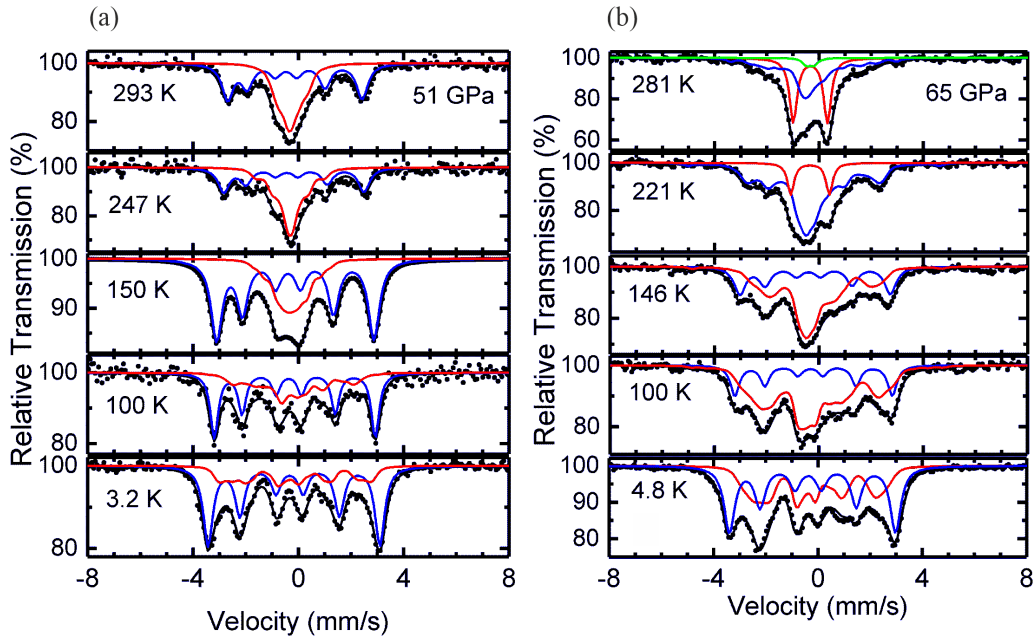

FIG. 9. Temperature dependence of the SMS spectra at (a) 51 GPa and (b) 65 GPa. Dots correspond to the experimental data, solid lines are the calculated spectra, and colored lines correspond to the subspectra.

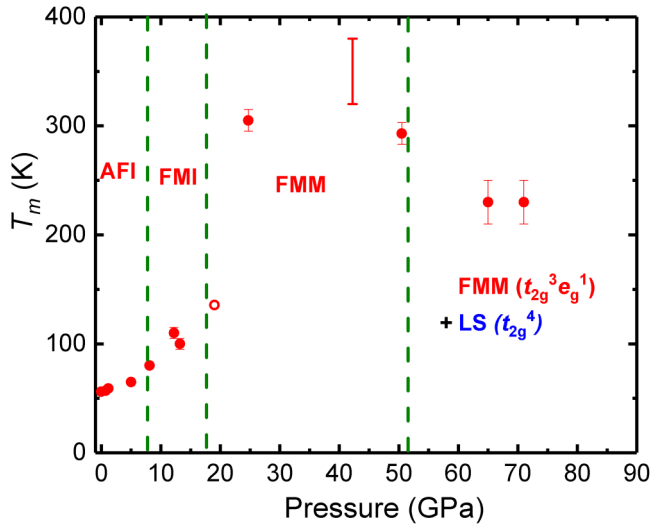

FIG. 10. Magnetic phase diagram of Sr_2FeO_4 at high pressures based on the present data and those of Ref. [38]. Below 8 GPa the system is insulating and adopts a spiral antiferromagnetic state (AFI), between 8 and 18 GPa the ground state is still insulating (semiconductor with a small gap) but ferromagnetic (FMI), and between 18 and ∼50 GPa a ferromagnetic metallic (FMM) state occurs with enhanced magnetic ordering temperature T_m. At 42 GPa, T_m is above RT and cannot be determined from the present data which is indicated by a bar tentatively marking a range of possible T_m. Beyond 50 GPa, T_m decreases again and phase coexistence of the FMM state with a low-spin (LS) state emerges beyond 50 GPa due to a partial HS→LS transition. The AFI, FMI, and FMM states are related to the HS $t_{2g}^3e_g^1$ electron configuration, while the LS state (blue) corresponds to a t_{2g}^4 configuration. The dashed green lines separate the regions of different electronic/magnetic behavior. The open symbol corresponds to a data point from Ref. [38].

for both components. The spectra and Mössbauer parameters obtained at nominal pressures of 65 and 71 GPa are quite similar. Considering the small beam size and nonhydrostatic pressure conditions at such high pressures, the local pressures in the small volumes probed by the SMS beam could have been quite similar in the two measurement series. Pressure inhomogeneities may also be at least partly the origin for the broad temperature ranges featuring phase coexistence. Nevertheless, the 89-GPa spectrum revealed the smallest IS [Fig. 5(b)], which indicates that in this run indeed the highest pressure was generated.

IV. DISCUSSION

A. Magnetic phase diagram

The results of the present high-pressure studies of Sr_2FeO_4, including results from the previous study [38], are summarized in a magnetic (P,T) phase diagram depicted in Fig. 10. Up to about 7 GPa, Sr_2FeO_4 exhibits an insulating antiferromagnetic ground state that may be stabilized by a hidden Jahn-Teller (JT) -like structural instability [37]. The latter could be the origin for an unexpected oxygen-derived phonon mode observed in Raman spectra [36,16]. Competing exchange interactions together with anisotropy result in an elliptical cycloidal spin modulation [16]. The additional Raman band disappears near 6 GPa, and between 7 and 8 GPa the spin structure changes to a ferromagnetic one. Thus, it is likely that the change in spin structure is correlated with the suppression of the supposed structural instability and formation of the undistorted *I*4/*mmm* crystal structure. A structural change is also supported by a minimum in QS at RT near 5 GPa as reported by Rozenberg *et al.* [38] and confirmed in the present study [Fig. 5(b)]. Electrical resistance studies indicated that in this pressure range a larger gap is closed, but the compound still remains semiconducting [38]. Metallization is expected near 18 GPa and a drastic enhancement in T_m occurs beyond 20 GPa which exceeds room temperature between about 25 and 50 GPa. Although we have not studied the magnetism in this pressure range by field dependent SMS, it is likely that between 20 and 50 GPa, Sr_2FeO_4 is in a FMM state.

Drastic changes in the SMS spectra indicate that between 50 and 90 GPa a phase transition occurs. The most striking feature is the emergence of a quadrupole doublet with a large QS of about 1.2 mm/s near RT which seems to be the single component in the RT spectrum at 89 GPa. The large QS indicates a large structural distortion around the Fe^{4+} ion and/or an electronic contribution to the EFG, which most likely is the signature of a pressure-induced HS→LS transition. A HS→LS transition changes the electron configuration from $t_{2g}^3e_g^1$ (referring to octahedral notation) with $S = 2$ to t_{2g}^4 with $S = 1$. Splitting of the t_{2g} orbitals by the lower-symmetry ligand field components leads to an unequal population of orbitals which can result in a valence contribution to the EFG. The reduction of the spin from $S = 2$ to $S = 1$ is in agreement with the decrease in T_m. The present changes in the SMS spectra at RT are reminiscent of those reported for *A*-site ordered perovskite type ferrates where HS→LS transitions are well documented [33,34]. Unfortunately, the SMS spectra of Sr_2FeO_4 beyond 50 GPa correspond to phase mixtures and the complex low-temperature spectra could not be decomposed into well-defined components. Pressure inhomogeneity and failure of the diamond anvils at 89 GPa hindered more unambiguous clues. More detailed SMS studies with careful pressure control and investigations of the crystal structure of Sr_2FeO_4 beyond 50 GPa are required to clarify the structural details and detailed magnetic behavior in the pressure range of the anticipated HS→LS transition.

B. Electronic structure considerations

Recently Kazemi-Moridani *et al.* reported a theoretical study on the ambient and high-pressure electronic state of Sr_2FeO_4 using a combination of DFT and DMFT [39]. The electronic properties were discussed within an effective orbital model based on the t_{2g} and e_g orbitals in terms of Mott and Hund's physics that is governed by the relative magnitude of the Coulomb repulsion U and Hund's rule coupling J. The study considered only the nonmagnetic state and compiled an electronic phase diagram in the J-U space at a temperature of 146 K. A main clue from the study was that the insulator-metal transition at 18 GPa leads to the formation of a metallic state where conduction takes place only within the t_{2g} orbitals while the e_g orbitals were considered to be empty. Thus, Sr_2FeO_4 would be in the LS (t_{2g}^4) state above 18 GPa. In particular, the

correlated band structure of Sr_2FeO_4 at 40 GPa was compared with that of Sr_2RuO_4 at ambient pressure and remarkable similarities were found, suggesting that Sr_2FeO_4 in this pressure range could exhibit similar low-energy properties [39]. Their interpretation was based on an estimated parameter regime $U \geqslant 2.5$ eV and $J < 0.7$ eV in order to explain the insulating ground state of Sr_2FeO_4. It was assumed that the *I*4/*mmm* crystal structure is retained in the whole pressure range.

The present experimental study reveals that Sr_2FeO_4 is magnetically ordered beyond 20 GPa with T_m even exceeding RT at 40 GPa. Such a high T_m in a layered system is difficult to reconcile with a t_{2g}^4 LS configuration. A photoemission study of $SrFeO_3$ has verified that at ambient pressure the Fe^{4+} ions adopt a high-spin ground state [4] and considering the similar average bond distances [35] as well as the Mössbauer parameters and magnetic properties of Sr_2FeO_4 [12,13] there are no indications that the spin state of Sr_2FeO_4 differs from that of $SrFeO_3$. In terms of the multiorbital model of Ref. [39] we suggest a different scenario starting from the formal $t_{2g}^3 e_g^1$ HS electron configuration and assign the metallic state of Sr_2FeO_4 beyond 18 GPa rather to the t_{2g} Mott insulator state of Ref. [39], where the e_g electrons are metallic and which is characterized by a large Hund's coupling $J \geqslant 0.8$ eV. It is emphasized that actually the t_{2g} and e_g orbitals are molecular orbitals with large O 2*p* contributions owing to the strongly covalent Fe-O bonds in high oxidation state TM oxides (cf. the negative-Δ scenario discussed in the Introduction). The FMM state above 18 GPa then arises from the double-exchange (DE) -like coupling of the itinerant e_g electrons with the localized t_{2g} orbitals. The insulating state of Sr_2FeO_4 in the low-pressure region possibly is rather stabilized by breaking of the *I*4/*mmm* symmetry leading to a gap within the e_g levels. This suggestion is supported by the unexpected Raman phonon [36,16] as well as by the recent theoretical prediction of a JT type instability [37]. It is noted that it can be challenging to verify such an instability in a layered system by diffraction methods [11]. Owing to the increase in the bandwidth of the e_g levels under pressure, the structural instability is removed above 6 GPa and the system finally metallizes at 18 GPa. The metallization of the e_g levels is reflected in a corresponding drop of B_{hf} [Fig. 5(a)] as the magnetic moment contribution of the e_g levels is lost. Most remarkably, the electronic ground state remains insulating up to 18 GPa. The persistence of local JT fluctuations between 6 and 18 GPa could prevent full metallization in this pressure region. Similar observations were reported for the metallization process of $LaMnO_3$, where the Mn^{3+} ion is JT active too and isoelectronic to the Fe^{4+} ion [50,51].

Further pressure increase leads to two opposing effects, namely, an increase in the e_g bandwidth but also to an enhanced ligand field splitting between the t_{2g} and e_g electrons owing to the decrease in Fe-O bond lengths. As discussed above, in the case of $3d^4$ ions a HS→LS transition may emerge which has been suggested to occur in $CaFeO_3$ [30], a perovskite compound adopting a monoclinic crystal structure and CD of Fe^{4+} at ambient pressure. In the case of $SrFeO_3$ the FMM state persists up to 74 GPa without indications for a *P*-driven HS→LS transition [26]. For the lower-dimensional Sr_2FeO_4 featuring a smaller e_g bandwidth than $SrFeO_3$, our SMS spectra indicate a HS→LS transition beyond ∼60 GPa, the details of which need to be explored in further studies. In conclusion, contrary to Ref. [39] the t_{2g}^4 LS state is rather expected above 60 GPa, while the FMM state between 18 and 50 GPa is related to itinerant e_g electrons.

C. Comparison with related iron(IV) oxides

We now compare the *P*-dependent electronic and magnetic behavior of Sr_2FeO_4, $Sr_3Fe_2O_7$, and $SrFeO_3$ which are the $n = 1$, 2, and ∞ members of the Ruddlesden-Popper series $Sr_{n+1}Fe_nO_{3n+1}$. At ambient pressure all the compounds adopt an incommensurate spiral spin structure with comparable propagation vector [14,9,15,16]. The insulating state in $Sr_3Fe_2O_7$ is stabilized by a CD of Fe(IV) and, as discussed above, there are indications that the insulating state of Sr_2FeO_4 is stabilized by a structural instability too. While $SrFeO_3$ is already metallic at ambient pressure, Sr_2FeO_4 and $Sr_3Fe_2O_7$ exhibit metallization at pressures around 20 GPa, and the low-*T* instabilities are suppressed owing to the increasing bandwidth of the e_g levels. For $SrFeO_3$ and Sr_2FeO_4 it has been verified by the detailed Mössbauer studies in external magnetic fields that the spiral antiferromagnetic spin structures in the low-*P* regime are transformed to FM spin structures above 7 GPa. In the FMM regime T_m is strongly enhanced in both compounds and exceeds RT. A peculiarity of Sr_2FeO_4 is that it adopts a semiconducting FM state between 7 and 18 GPa with a moderate increase in T_m with increasing *P*. Details of the (*P*,*T*) diagram of $Sr_3Fe_2O_7$ have not been reported yet but the CD of Fe(IV) is suppressed near 20 GPa and a single six-line pattern is observed in the Mössbauer spectra of the magnetically ordered phase above 20 GPa [32]. It is likely that beyond 20 GPa, $Sr_3Fe_2O_7$ enters the FMM state too.

The (*P*,*T*) phase diagram of Sr_2FeO_4 depicted in Fig. 10 bears remarkable similarities to the (*P*,*T*) phase diagrams of the *A*-site ordered Fe(IV) perovskites $ACu_3Fe_4O_{12}$ (A = Ca, Sr) [33,34]. In these compounds the low-pressure CD state is suppressed near ∼15 GPa and an FMM state emerges with a nearly charge-uniform Fe^{4+} HS (essentially $t_{2g}^3 e_g^1$) configuration and with T_m above RT. Beyond 30 GPa, a well-defined HS→LS transition occurs which leads to a LS (t_{2g}^4) metallic state with a drastic reduction in T_m and symmetry lowering indicated by a quadrupole doublet in RT Mössbauer spectra. Compared to the *A*-site ordered perovskites the stability range of the FMM HS state is much broader for Sr_2FeO_4 and the HS→LS transition only emerges beyond 60 GPa.

The present and literature results suggest a generic (*P*,*T*) phase diagram that is similar for all the Fe(IV) perovskite-related oxides. Below a critical pressure P_1 the compounds adopt antiferromagnetic states and in the case of small e_g bandwidths insulating states are formed which are stabilized by a CD or JT type instability. Several of the compounds adopt spiral spin structures in the low-*P* range where the e_g electrons still have a considerable degree of localization. At pressures above P_1, a FMM HS state is formed which is characterized by high T_m values exceeding RT owing to DE-like coupling between the itinerant e_g and more localized t_{2g} levels. Beyond a second critical pressure P_2 a pressure-induced HS→LS transition occurs which leads to a FMM LS state with reduced T_m.

The values of P_1 and P_2 depend on the details of the system and it is anticipated that the critical pressures are governed by the interplay between structural details defining the electron hopping t and e_g bandwidth w, the Coulomb repulsion U, and the Hund's coupling J. Finally it is mentioned that similar (P,T) phase diagrams were also observed for formally mixed-valent $Fe^{3.75+}$ based ferrates [52,53].

V. CONCLUSIONS

We have investigated the pressure dependence of the electronic and magnetic state of the K_2NiF_4-type Fe(IV) oxide Sr_2FeO_4 up to 89 GPa by energy-domain synchrotron Mössbauer spectroscopy and derived a (P,T) magnetic phase diagram. Up to about 7 GPa, Sr_2FeO_4 is an insulator with an elliptically modulated spiral spin structure which at higher pressures is transformed into a semiconducting ferromagnetic state. Above 6 GPa a possibly Jahn-Teller type structural instability indicated by Raman spectra and theoretical predictions is suppressed, but local JT fluctuations may persist which could explain why the system remains semiconducting. According to Ref. [38], Sr_2FeO_4 metallizes near 18 GPa. Similar as in other Fe(IV) oxides, the magnetic ordering temperature in the ferromagnetic metallic regime is enhanced to beyond room temperature between 20 and 50 GPa. Between 50 and 89 GPa a decrease in magnetic ordering temperature and signatures for a high-spin to low-spin transition were found. Up to at least 50 GPa, the electronic properties are derived from the $t_{2g}^3 e_g^1$ high-spin configuration, which makes the metallic state of Sr_2FeO_4 in this pressure range distinct from that of Sr_2RuO_4 where metallic conduction is associated with the t_{2g} bands. However, it bears some analogy to the nickelate high-T_c superconductor $La_3Ni_2O_7$ where metallicity is associated with the e_g levels too [1]. Only beyond ~60 GPa can a metallic t_{2g}^4 state predicted in Ref. [39] be expected, which in contrast to Sr_2RuO_4 is still magnetically ordered. We hope that the present experimental investigations on the high-pressure behavior of Sr_2FeO_4, considerably extending the pressure range of the earlier study [38] and providing more details of the electronic/magnetic phase diagram, may stimulate refined theoretical studies of this interesting oxide and enable further comparison of its electronic structure with that of the superconductors Sr_2RuO_4 and $La_3Ni_2O_7$.

ACKNOWLEDGMENTS

We gratefully acknowledge the ESRF for granting beamtime at the Nuclear Resonance beamline ID18 under Proposals No. HC-4292 and No. HC-4728. We thank J.-P. Celse for technical assistance during the beamtimes at ID18.

[1] H. Sun, M. Huo, X. Hu, J. Li, Z. Liu, Y. Han, L. Tang, Z. Mao, P. Yang, B. Wang, J. Cheng, D.-X. Yao, G.-M. Zhang, and M. Wang, Signatures of superconductivity near 80 K in a nickelate under high pressure, Nature (London) **621**, 493 (2023).

[2] J. Zaanen, G. A. Sawatzky, and J. W. Allen, Band gaps and electronic structure of transition-metal compounds, Phys. Rev. Lett. **55**, 418 (1985).

[3] T. Mizokawa, H. Namatame, A. Fujimori, K. Akeyama, H. Kondoh, H. Kuroda, and N. Kosugi, Origin of the band gap in the negative charge-transfer-energy compound $NaCuO_2$, Phys. Rev. Lett. **67**, 1638 (1991).

[4] A. E. Bocquet, A. Fujimori, T. Mizokawa, T. Saitoh, H. Namatame, S. Suga, N. Kimizuka, Y. Takeda, and M. Takano, Electronic structure of $SrFe^{4+}O_3$ and related Fe perovskites, Phys. Rev. B **45**, 1561 (1992).

[5] S. Kitou, M. Gen, Y. Nakamura, K. Sugimoto, Y. Tokunaga, S. Ishiwata, and T.-h. Arima, Real space observation of ligand hole state in cubic perovskite $SrFeO_3$, Adv. Sci. **10**, 2302839 (2023).

[6] P. K. Gallagher, J. B. MacChesney, and D. N. E. Buchanan, Mössbauer effect in the system $SrFeO_{2.5-3.0}$, J. Chem. Phys. **41**, 2429 (1964).

[7] J. B. MacChesney, R. C. Sherwood, and J. F. Potter, Electrical and magnetic properties of the strontium ferrates, J. Chem. Phys. **43**, 1907 (1965).

[8] M. Takano, N. Nakanishi, Y. Takeda, S. Naka, and T. Takada, Charge disproportionation in $CaFeO_3$ studied with the Mössbauer effect, Mater. Res. Bull. **12**, 923 (1977).

[9] P. M. Woodward, D. E. Cox, E. Moshopoulou, A. W. Sleight, and S. Morimoto, Structural studies of charge disproportionation and magnetic order in $CaFeO_3$, Phys. Rev. B **62**, 844 (2000).

[10] K. Kuzushita, S. Morimoto, S. Nasu, and S. Nakamura, Charge disproportionation and antiferromagnetic order of $Sr_3Fe_2O_7$, J. Phys. Soc. Jpn. **69**, 2767 (2000).

[11] J.-H. Kim, D. C. Peets, M. Reehuis, P. Adler, A. Maljuk, T. Ritschel, M. C. Allison, J. R. L. Mardegan, J. Geck, P. J. Bereciartua Perez, S. Francoual, A. C. Walters, T. Keller, P. M. Abdala, P. Pattison, P. Dosanjh, and B. Keimer, Hidden charge order in an iron oxide square lattice compound, Phys. Rev. Lett. **127**, 097203 (2021).

[12] S. E. Dann, M. T. Weller, D. B. Currie, M. F. Thomas, and A. D. Al-Rawwas, Structure and magnetic properties of Sr_2FeO_4 and $Sr_3Fe_2O_7$ studied by powder neutron diffraction and Mössbauer spectroscopy, J. Mater. Chem. **3**, 1231 (1993).

[13] P. Adler, Properties of K_2NiF_4-type oxides $Sr_2FeO_{\sim 4}$, J. Solid State. Chem. **108**, 275 (1994).

[14] T. Takeda, Y. Yamaguchi, and H. Watanabe, Magnetic structure of $SrFeO_3$, J. Phys. Soc. Jpn. **33**, 967 (1972).

[15] J.-H. Kim, A. Jain, M. Reehuis, G. Khaliullin, D. C. Peets, C. Ulrich, J. T. Park, E. Faulhaber, A. Hoser, H. C. Walker *et al.*, Competing exchange interactions at the verge of a metal-insulator transition in the two-dimensional spiral magnet $Sr_3Fe_2O_7$, Phys. Rev. Lett. **113**, 147206 (2014).

[16] P. Adler, M. Reehuis, N. Stüßer, S. A. Medvedev, M. Nicklas, D. C. Peets, J. Bertinshaw, C. K. Christensen, M. Etter, A. Hoser, L. Schröder, P. Merz, W. Schnelle, A. Schulz, Q. Mu, D. Bessas, A. Chumakov, M. Jansen, and C. Felser, Spiral magnetism, spin flop, and pressure-induced ferromagnetism in the negative charge-transfer-gap insulator Sr_2FeO_4, Phys. Rev. B **105**, 054417 (2022).

[17] Y. Tokura and N. Kanazawa, Magnetic skyrmion materials, Chem. Rev. **121**, 2857 (2021).

[18] S. Chakraverty, T. Matsuda, H. Wadati, J. Okamoto, Y. Yamasaki, H. Nakao, Y. Murakami, S. Ishiwata, M. Kawasaki, Y. Taguchi, Y. Tokura, and H. Y. Hwang, Multiple helimagnetic phases and topological Hall effect in epitaxial thin films of pristine and Co-doped $SrFeO_3$, Phys. Rev. B **88**, 220405(R) (2013).

[19] S. Ishiwata, T. Nakajima, J.-H. Kim, D. S. Inosov, N. Kanazawa, J. S. White, J. L. Gavilano, R. Georgii, K. M. Seemann, G. Brandl *et al.*, Emergent topological spin structures in the centrosymmetric cubic perovskite $SrFeO_3$, Phys. Rev. B **101**, 134406 (2020).

[20] N. D. Andriushin, J. Grumbach, J. H. Kim, M. Reehuis, Y. V. Tymoshenko, Y. A. Onykiienko, A. Jain, W. A. MacFarlane, A. Maljuk, S. Granovsky, A. Hoser, V. Pomjakushin, J. Ollivier, M. Doerr, B. Keimer, D. S. Inosov, and D. C. Peets, Rich magnetic phase diagram of the putative helimagnet $Sr_3Fe_2O_7$, Phys. Rev. B **108**, 174420 (2023).

[21] M. Mostovoy, Helicoidal ordering in iron perovskites, Phys. Rev. Lett. **94**, 137205 (2005).

[22] S. Nasu, T. Abe, K. Yamamoto, S. Endo, M. Takano, and Y. Takeda, ^{57}Fe Mössbauer study of $SrFeO_3$ under ultra-high pressure, Hyperfine Interact. **67**, 529 (1991).

[23] S. Nasu, K. Wada, T. Abe, K. Yamamoto, S. Endo, M. Takano, and Y. Takeda, High-pressure Mössbauer study of perovskite iron oxides, Nucl. Instrum. Methods Phys. Res., Sect. B **76**, 185 (1993).

[24] S. Nasu, High-pressure Mössbauer spectroscopy with nuclear forward scattering of synchrotron radiation, High Press. Res. **14**, 405 (1996).

[25] S. Nasu, High pressure experiments with synchrotron radiation, Hyperfine Interact. **113**, 97 (1998).

[26] S. Nasu, High-pressure Mössbauer spectroscopy using synchrotron radiation and radioactive sources, Hyperfine Interact. **128**, 101 (2000).

[27] S. Nasu, T. Kawakami, S. Kawasaki, and M. Takano, High-pressure Mössbauer spectroscopy of perovskite iron oxides, Hyperfine Interact. **144**, 119 (2002).

[28] T. Kawakami and S. Nasu, High-pressure Mössbauer spectroscopy of perovskite high valence iron oxides under external magnetic field, J. Phys.: Condens. Matter **17**, S789 (2005).

[29] T. Kawakami, S. Nasu, K. Kuzushita, T. Sasaki, S. Morimoto, T. Yamada, S. Endo, S. Kawasaki, and M. Takano, High-pressure Mössbauer and x-ray powder diffraction studies of $SrFeO_3$, J. Phys. Soc. Jpn. **72**, 33 (2003).

[30] M. Takano, S. Nasu, T. Abe, K. Yamamoto, S. Endo, Y. Takeda, and J. B. Goodenough, Pressure-induced high-spin to low-spin transition in $CaFeO_3$, Phys. Rev. Lett. **67**, 3267 (1991).

[31] T. Kawakami, S. Nasu, T. Sasaki, S. Morimoto, S. Endo, S. Kawasaki, and M. Takano, Charge disproportionation and magnetic order of $CaFeO_3$ under high pressure up to 65 GPa, J. Phys. Soc. Jpn. **70**, 1491 (2001).

[32] P. Adler, U. Schwarz, K. Syassen, G. K. Rozenberg, G. Y. Machavariani, A. P. Milner, M. P. Pasternak, and M. Hanfland, Collapse of the charge disproportionation and covalency-driven insulator-metal transition in $Sr_3Fe_2O_7$ under pressure, Phys. Rev. B **60**, 4609 (1999).

[33] T. Kawakami, Y. Sekiya, A. Mimura, K. Kobayashi, I. Yamada K.Tokumichi, M. Mizumaki, N. Kawamura, Y. Shimakawa, Y. Ohishi, N. Hirao, N. Ishimatsu, N. Hayashi, and M. Takano, Two-step suppression of charge disproportionation in $CaCu_3Fe_4O_{12}$ under high pressure, J. Phys. Soc. Jpn. **85**, 034716 (2016).

[34] T. Kawakami, A. Mimura, M. Ishii, Y. Watanabe, Y. Nakakura, and I. Yamada, Pressure-induced intersite charge transfer in $SrCu_3Fe_4O_{12}$, J. Phys. Soc. Jpn. **88**, 064704 (2019).

[35] S. E. Dann, M. T. Weller, and D. B. Currie, Synthesis and structure of Sr_2FeO_4, J. Solid State. Chem. **92**, 237 (1991).

[36] P. Adler, A. F. Goncharov, K. Syassen, and E. Schönherr, Optical reflectivity and Raman spectra of Sr_2FeO_4 under pressure, Phys. Rev. B **50**, 11396 (1994).

[37] G. Zvejnieks, Y. Mastrikov, and D. Gryaznov, Jahn-Teller distortion in Sr_2FeO_4: Group theoretical analysis and hybrid DFT calculations, Sci. Rep. **13**, 16446 (2023).

[38] G. Kh. Rozenberg, A. P. Milner, M. P. Pasternak, G. R. Hearne, and R. D. Taylor, Experimental confirmation of a *p-p* intraband gap in Sr_2FeO_4, Phys. Rev. B **58**, 10283 (1998).

[39] A. Kazemi-Moridani, S. Beck, A. Hampel, A.-M. S. Tremblay, M. Coté, and O. Gingras, Strontium ferrite under pressure: Potential analog to strontium ruthenate, Phys. Rev. B **109**, 165146 (2024).

[40] V. Potapkin, A. I. Chumakov, G. V. Smirnov, J.-P. Celse, R. Rüffer, C. McCammon, and L. Dubrovinski, The ^{57}Fe synchrotron Mössbauer source at the ESRF, J. Synchrotron Radiat. **19**, 559 (2012).

[41] R. Rüffer and A. I. Chumakov, Nuclear-resonance beamline at ESRF, Hyperfine Interact. **97**, 589 (1996).

[42] Z. Klencsár, E. Kuzmann, and A. Vértes, User-friendly software for Mössbauer spectrum analysis, J. Radioanal. Nucl. Chem. **210**, 105 (1990).

[43] M. E. Matsnev and V. S. Rusakov, Study of spatial-spin-modulated structures by Mössbauer spectroscopy using SpectrRelax, AIP Conf. Proc. **1622**, 40 (2014).

[44] S. Yaroslavtsev, SYNCmoss software package for fitting Mössbauer spectra measured with a synchrotron Mössbauer source, J. Synchrotron Radiat. **30**, 596 (2023).

[45] See Supplemental Material at http://link.aps.org/supplemental/10.1103/PhysRevB.110.054444 for Raman spectra, additional SMS spectra, and more details about the evaluation of some of the SMS spectra with the ASM model.

[46] D. Colson, A. Forget, and P. Bonville, The modulated antiferromagnetic structures in multiferroic $FeVO_4$: A ^{57}Fe Mössbauer spectroscopy investigation, J. Magn. Magn. Mater. **378**, 529 (2015).

[47] A. Palewicz, T. Szumiata, K. Przeniosło, I. Sonowska, and I. Margiolaki, Search for new modulations in the $BiFeO_3$ structure: SR diffraction and Mössbauer studies, Solid State Commun. **140**, 359 (2006).

[48] V. S. Rusakov, V. S. Pakatilov, A. S. Sigov, M. E. Matsnev, and T. V. Gubaidulina, Diagnostics of a spatial spin-modulated structure using nuclear magnetic resonance and Mössbauer spectroscopy, JETP Lett. **100**, 463 (2014).

[49] V. S. Rusakov, V. S. Pokatilov, A. S. Sigov, M. E. Matsnev, A. M. Gapochka, and A. P. Pyatakov, The effect of temperature on parameters of hyperfine interactions and spatial spin-modulated structure in multiferroic $BiFeO_3$, Ferroelectrics **569**, 286 (2020).

[50] I. Loa, P. Adler, A. Grzechnik, K. Syassen, U. Schwarz, M. Hanfland, G. Kh. Rozenberg, P. Korodetsky, and M. P. Pasternak, Pressure-induced quenching of the Jahn-Teller distortion and insulator-to-metal transition in $LaMnO_3$, Phys. Rev. Lett. **87**, 125501 (2001).

[51] D. P. Kozlenko, E. V. Lukin, S. E. Kichanov, Z. Jirák, N. O. Golosova, and B. N. Savenko, High-pressure evolution of the magnetic order in $LaMnO_3$, Phys. Rev. B **107**, 144426 (2023).

[52] T. Kawakami, S. Nasu, T. Sasaki, K. Kuzushita, S. Morimoto, S. Endo, T. Yamada, S. Kawasaki, and M. Takano, Pressure-induced transformation from a charge-disproportionated antiferromagnetic state to a charge-uniform ferromagnetic state in $Sr_{2/3}La_{1/3}FeO_3$, Phys. Rev. Lett. **88**, 037602 (2002).

[53] T. Kawakami, Y. Nakakura, K. Tokumichi, Y. Ohishi, N. Hirao, and I. Yamada, Pressure-induced spin transition in $LuCu_3Fe_4O_{12}$, J. Phys. Soc. Jpn. **91**, 054708 (2022).